Mineral Dissolution Kinetics at the Pore Scale

Li Li, Carl I. Steefel, Li Yang

Earth Sciences Division
Lawrence Berkeley National Laboratory
1 Cyclotron Road, MS 90-1116
Berkeley, CA 94720

Abstract

Mineral dissolution rates in the field have been reported to be orders of magnitude slower than those measured in the laboratory, an unresolved discrepancy that severely limits our ability to develop scientifically defensible predictive or even interpretive models for many geochemical processes in the earth and environmental sciences. One suggestion links this discrepancy to the role of physical and chemical heterogeneities typically found in subsurface soils and aquifers in producing scale-dependent rates where concentration gradients develop. In this paper, we examine the possibility that scale-dependent mineral dissolution rates can develop even at the single pore and fracture scale, the smallest and most fundamental building block of porous media. To do so, we develop two models to analyze mineral dissolution kinetics at the single pore scale: 1) a Poiseuille Flow model that applies laboratory-measured dissolution kinetics at the pore or fracture wall and couples this to a rigorous treatment of both advective and diffusive transport, and 2) a Well-Mixed Reactor model that assumes complete mixing within the pore, while maintaining the same reactive surface area, average flow rate, and geometry as the Poiseuille Flow model. For a fracture, a 1D Plug Flow Reactor model is considered in addition to quantify the effects of longitudinal versus transverse mixing. The comparison of averaged dissolution rates under various conditions of flow, pore size, and fracture length from the three models is used as a means to quantify the extent to which concentration gradients at the single pore and fracture scale can develop and render rates scale-dependent. Three important minerals that dissolve at widely different rates, calcite, plagioclase, and iron hydroxide, are considered. The modeling indicates that rate discrepancies arise primarily where concentration gradients develop due to comparable rates of reaction and advective transport, and incomplete mixing via molecular diffusion. The magnitude of the reaction rate is important, since it is found that scaling effects (and thus rate discrepancies) are negligible at the single pore and fracture scale for plagioclase and iron hydroxide because of the slow rate at which they dissolve. In the case of calcite, where dissolution rates are rapid, scaling effects can develop at high flow rates from 0.1 cm/s to 1000 cm/s and for fracture lengths less than 1 cm. At more normal flow rates, however, mixing via molecular diffusion is effective in homogenizing the concentration field, thus eliminating any discrepancies between the Poiseuille Flow and the Well-Mixed Reactor model. This suggests that a scale dependence to mineral dissolution rates is unlikely at the single pore or fracture scale under normal geological/hydrologic conditions, implying that the discrepancy between laboratory and field rates must be attributed to other factors.

1. Introduction

The dissolution of minerals plays a major role in various physical, chemical, and biological processes in nature. Mineral dissolution affects the formation of soils, influences the degradation of radioactive waste and its containers (SPYCHER et al., 2003) and the subsequent migration of heavy metals and radionuclides to the biosphere (CHOROVER et al., 2003; LOVLEY, 1993; LOVLEY and COATES, 1997), and at larger space and time scales, it regulates the atmospheric concentrations of CO_2 (BERNER, 1995; BERNER and BERNER, 1997). Laboratory-measured dissolution rates of many minerals have been consistently found to be several orders of magnitude faster than those observed in the field (MAHER et al., 2004; WHITE and BRANTLEY, 2003), although it is not clear in all cases that this represents a true discrepancy in the rate constants as opposed to a failure to take into account the intrinsic differences in chemical and/or physical conditions between laboratory and field settings (STEEFEL et al., 2005). Such rate discrepancies need to be resolved, however, since they seriously hinder the application of laboratory-measured dissolution rates to natural systems.

A variety of factors have been proposed to contribute to the rate discrepancy, including the differences in reactive surface area of the fresh and weathered minerals (ANBEEK, 1993; WHITE, 1995; WHITE and PETERSON, 1990), the effect of reaction affinity (MAHER et al., 2006; WHITE, 1995; WHITE and BRANTLEY, 2003), the precipitation rate of secondary clay minerals (ALEKSEYEV et al., 1997; MAHER et al., 2006; STEEFEL and VAN CAPPELLEN, 1990; ZHU et al., 2004), and the age of the reacting material (MAHER et al., 2004; WHITE and BRANTLEY, 2003). Recent studies have also shown that physical and chemical heterogeneities in soils and aquifers where subsurface flow occurs may contribute to a scale dependence to mineral dissolution rates, and thus potentially to discrepancies between laboratory and field rates (LI et al., 2006; MALMSTROM et al., 2000; MALMSTROM et al., 2004; MEILE and TUNCAY, 2006). For example, Li and coworkers (LI et al., 2006; LI et al., 2007) found that variations in the spatial distributions of minerals with differing reactivities can result in the development of concentration gradients of chemical species involved in dissolution reactions, thus leading to erroneous predictions of reaction rates when the scale dependence is not accounted for. More generally, any chemical, physical, or microbiological heterogeneity that results in the formation of concentration gradients in the subsurface can lead to a scale dependence to the rates, and thus potentially to discrepancies between laboratory and field rates.

While the discrepancies between laboratory and field rates cannot be attributed entirely to the effect of physical and chemical heterogeneities, as indicated by studies of weathering rates in physically and chemically homogeneous media (MAHER et al., 2006), it is clear that a comparison of lab and field rates requires careful consideration of the inherent differences between the laboratory and natural systems as suggested above. The laboratory measurement of dissolution rates usually employs well-mixed batch or flow through reactors. In these experimental systems, the aqueous phase is stirred rapidly enough that the aqueous phase becomes well-mixed, thus eliminating the effect of transport. In such cases, mineral dissolution is surface-controlled and depends only on the uniform chemistry of the aqueous solution. In natural systems, however, reactions are inevitably subject to the influence of transport via advection, molecular diffusion, and/or dispersion. As such, the mineral dissolution rates are an

outcome of coupling between the reaction and transport processes, in contrast to the solely "reactive" processes characterizing well-mixed laboratory systems.

In addition to these differences, natural porous or fractured media are also very different from laboratory settings in terms of their structure and heterogeneous nature. For example, natural porous media typically possess hierarchical structures and spatial scales that range from the pore scale, to the continuum scale, and finally to the field scale. The pore scale focuses on individual pores at the spatial scale of tens to thousands of microns, while the continuum scale, often at the scale of millimeters to centimeters, contains a sufficient number of pores that allows the definition of statistically averaged properties of porous media, including porosity and permeability (BEAR, 1972). The field scale, often from meters to kilometers, is the scale at which we examine specific processes in natural field settings. Heterogeneities in the physical and chemical properties of porous media exist at all spatial scales. While at the continuum and field scales porous media are often represented by properties and processes "averaged" over a large number of pores, pore scale are where processes such as flow, transport, and reactions actually take place. As such, pores are the fundamental building blocks of natural porous media and are an important starting point to examine the scaling issue with regard to reaction rates.

In this work, we focus on mineral dissolution in single pores and fractures, where flow can no longer be described completely by an average Darcy velocity—gradients in flow velocity inevitably exist within individual pores as a result of the fundamental physics. Such flow gradients, as well as the limited rates of diffusive transport, can present conditions where reactions are limited by flow and transport, which are very different from conditions in well-mixed batch or flow through reactors in laboratory settings. In this work, laboratory-measured reaction kinetics is applied at the scale of the mineral-water interface where they occur, and then coupled with a rigorous representation of flow and transport in single pores and fractures. Although the model for a single pore is highly idealized in terms of its geometry, first order effects in terms of the coupling of flow, transport, and reaction kinetics are captured. We compare rates from these fully coupled reactive transport systems to those rates obtained from well-mixed reactors that ignore the effects of flow and transport, with such comparisons used to quantify the effects of flow and transport on mineral dissolution rates in natural systems at the pore scale. For single fractures, we compare the rates from fully coupled reactive transport systems to those calculated from 1D plug flow reactor model that assumes complete transverse mixing so as to evaluate its effect. The comparisons were made under various flow, pore size, and fracture length conditions to understand the mechanisms that contribute to the rate discrepancies between laboratory and field settings, and to identify the conditions under which such rate discrepancies become significant.

2. Reactions and rate laws

In this work we focus on the dissolution of three important subsurface mineral phases with a range of reaction rates: calcite, plagioclase, and iron hydroxide. Calcite dissolution is one of the most important and rapid mineral reactions in the subsurface (MORSE and ARVIDSON, 2002), while plagioclase dissolution is one of the slowest, its rate constant about 5-6 orders of magnitude less than that of calcite (BLUM and STILLINGS, 1995; WHITE and BRANTLEY, 1995). Dissimilatory iron reduction is an example of a dissolution reaction with an intermediate rate,

and is one of the most important biogeochemical reactions in the environment where it affects nutrient cycling and the fate of many subsurface contaminants (ANDERSON et al., 2003; COATES and ANDERSON, 2000; LOVLEY and COATES, 1997).

2.1 Calcite dissolution

The dissolution of calcite has been proposed to occur via three parallel reactions (CHOU et al., 1989; PLUMMER et al., 1978):

$$CaCO_3(s) + H^+ \rightleftharpoons Ca^{2+} + HCO_3^- \quad (1)$$

$$CaCO_3(s) + H_2CO_3^* \rightleftharpoons Ca^{2+} + 2HCO_3^- \quad (2)$$

$$CaCO_3(s) \rightleftharpoons Ca^{2+} + CO_3^{2-} \quad (3)$$

The reaction consumes H^+, and releases Ca^{2+} and carbonate. In the model, the rate of calcite dissolution is described by a Transition State Theory (TST) rate law, with the reaction rate parameters determined by (CHOU et al., 1989):

$$Rate = A(k_1 a_{H^+} + k_2 a_{H_2CO_3^*} + k_3)\left(1 - \frac{IAP}{K_{eq}}\right), \quad (4)$$

where k_1, k_2, and k_3 are the reaction rate constants, a_{H^+} and $a_{H_2CO_3^*}$ are the activities of hydrogen ion and carbonic acid, *IAP* and K_{eq} are the ion activity product and the equilibrium constant for the reaction respectively, and A is the reactive surface area. The values of k_1, k_2, and k_3 are 0.89, 5.01×10^{-4}, and 6.6×10^{-7} mol m^{-2} s^{-1}, respectively (CHOU et al., 1989). With this rate law, the reaction rate is pH dependent under acidic conditions and becomes almost constant above a pH of about 7 (Figure 2 in (CHOU et al., 1989)).

2.2 Plagioclase dissolution

Our model plagioclase contains 70% anorthite (labradorite), which dissolves under slightly acidic conditions according to the following reaction

$$Ca_{0.7}Na_{0.3}Al_{1.7}Si_{2.3}O_8 + 1.2H_2O + 6.8H^+ \rightleftharpoons 0.7Ca^{2+} + 0.3Na^+ + 1.7Al^{3+} + 2.3H_4SiO_4 \quad (5)$$

The dissolution of plagioclase has been described by several rate laws in the literature. In this work, we consider two separate rate laws. The first is an aluminum inhibition rate law (OELKERS et al., 1994) that describes the rate dependence on pH and aluminum concentration,

$$Rate = Ak\left(\frac{K_f'}{a_{Al(OH)_3}^{1/3} + K_f'}\right)\left(1 - \left(\frac{IAP}{K_{eq}}\right)^{1/3}\right), \quad (6)$$

here rewritten slightly following MAHER et al (2006). In Equation (6), K_f' is the formation constant for a silica-rich surface complex involved in the rate-limiting step in the overall dissolution reaction, which has a value of 1.50×10^{-5}. The rate constant for plagioclase

containing 70% anorthite is estimated to be 1.12×10^{-9} mol m^{-2} s^{-1}, which is extrapolated from a rate constant measured for a plagioclase containing 60% anorthite (CARROLL and KNAUSS, 2005) using a correlation between reaction rate constants and plagioclase composition (BLUM and STILLINGS, 1995). The equilibrium constant is 19.28 for a plagioclase that contains 70% anorthite (STEFANSSON, 2001).

The second rate law considered is one proposed by HELLMANN and TISSERAND (2006) that describes the dependence of the rate on reaction affinity or Gibbs free energy, and is very similar to one proposed earlier by BURCH et al (1993) for albite. This dependence is combined with the pH dependence described in BLUM and STILLINGS (1995) under far from equilibrium conditions. For a Ca-rich plagioclase, the rate dependence on pH is raised to the power of 0.72, giving the following overall reaction rate law:

$$Rate = \left\{ k_1 {a_{H^+}}^{0.72} [1-\exp(-ng^{m_1})] + k_2 {a_{H^+}}^{0.72} [1-\exp(-g)]^{m_2} \right\} A , \qquad (7)$$

where g is equal to $\left|\Delta G_r\right|/RT$, with ΔG_r being the Gibbs free energy of the reaction, R the gas constant, and T the temperature in degrees Kelvin. The parameters k_1 and k_2 are reaction rate constants estimated to be 5.01×10^{-8} and 8.69×10^{-10} mol m^{-2} s^{-1}, respectively, based on the plagioclase dissolution rate under far from equilibrium conditions (BLUM and STILLINGS, 1995) and the ratios of these two values in HELLMANN and TISSERAND (2006), who measured the rates at 150 °C. The values of n, m_1, and m_2 are 7.98×10^{-5}, 3.81, and 1.17, respectively taken from HELLMANN and TISSERAND (2006).

2.3 Dissimilatory iron reduction

Assuming acetate as the electron donor, dissimilatory reductive dissolution of an iron hydroxide like goethite proceeds as follows:

$$FeOOH(s) + \frac{1}{8}CH_3COO^- + \frac{15}{8}H^+ \rightleftharpoons Fe^{2+} + \frac{1}{4}HCO_3^- + \frac{3}{2}H_2O . \qquad (8)$$

The dependence of the rate on acetate is usually described by a Monod term. For goethite, however, recent studies have shown that the rate of iron reduction also depends on the surface area and the concentration of surface sites available for reaction (JAISI et al., 2007; LIU et al., 2001; RODEN and ZACHARA, 1996), which can be reduced due to the adsorption of Fe(II) on the goethite surface (RODEN, 2004; RODEN and URRUTIA, 2002; RODEN et al., 2000). Accordingly, we use the following rate law that combines a dependence on acetate concentration and on available iron hydroxide surface sites:

$$Rate = V_{\max,Fe(III)} \frac{c_{acetate}}{K_{s,acetate} + c_{acetate}} [> FeOH]_{available} , \qquad (9)$$

where $V_{\max,Fe(III)}$ is the maximum surface-area-normalized rate of iron reduction, with a value of 1.655×10^{-6} mol (mole sites)$^{-1}$ s^{-1} (SCHEIBE et al., 2006), $c_{acetate}$ is the aqueous concentration of acetate (mol/L), $K_{s,acetate}$ is the half-saturation constant of acetate, with a value of 0.0001 mol/L

(SCHEIBE et al., 2006), and $[>FeOH]_{available}$ is the available surface site density of iron hydroxide in units of (mole sites) m^{-2}. The value of $[>FeOH]_{available}$ is equal to $[>FeOH_s]+[>FeOH_w]-[>FeOFe^+{}_s]-[>FeOFe^+{}_w]$, which is the summation of total strong and weak iron surface site densities ($[>FeOH_s]$ and $[>FeOH_w]$, respectively), subtracted by the densities of sites occupied by the adsorbed Fe(II) ($[>FeOFe^+{}_s]$ and $[>FeOFe^+{}_w]$). The density of strong and weak iron surface sites are taken as 9.27×10^{-8} and 3.70×10^{-6} (mol sites) m^{-2} (APPELO et al., 2002), respectively. The adsorption of Fe(II) on iron hydroxide surface is modeled using a surface complexation model based on the electrical double layer theory (DZOMBAK and MOREL, 1990), with parameters from APPELO et al (2002):

$$>FeOH_s+Fe^{2+}=>FeOFe^+_s \qquad \log K=-0.95, \tag{10}$$

$$>FeOH_w+Fe^{2+}=>FeOFe^+_w \qquad \log K=-2.98. \tag{11}$$

According to this rate law, as the Fe(II) concentration in solution increases with the progress of the reaction, the concentrations of the sorbed species $>FeOFe^+{}_s$ and $>FeOFe^+{}_w$ increase as well, thus effectively inhibiting the rate of dissolution.

3. Models for single pores and fractures

3.1. Model for a single pore

To analyze the scale dependence of mineral dissolution rates at the pore scale, we develop two models: 1) a Poiseuille Flow model that applies laboratory-measured dissolution kinetics at the pore or fracture wall and couples this to a rigorous treatment of both advective and diffusive transport, and 2) a Well-Mixed Reactor model that assumes complete mixing within the pore, while maintaining the same reactive surface area, average flow rate, and geometry as the Poiseuille Flow model. The Poiseuille Flow model is considered as the more realistic representation of the actual processes taking place in the pore, while the Well-Mixed Reactor model is used as a means of quantifying of the extent to which concentration gradients within a single pore affect the averaged reaction rates.

Poiseuille Flow model:

In this model, pores are assumed to be cylindrical. Assuming Poiseuille's equation for flow in a cylinder holds, the steady-state parabolic velocity distribution within the pore as a function of radial distance *r* can be calculated from (DAUGHERTY and FRANZINI, 1965)

$$u(r)=2U\left[1-\left(\frac{r}{R}\right)^2\right], \tag{12}$$

where *u(r)* is the local fluid velocity within the cylinder, U is the average flow velocity, and *R* is the radius of the cylinder. As such, the local flow is fastest at the radial center of the pore and slowest close to the pore wall.

In the model, dissolution occurs only at the pore wall, which is made up of one of the three minerals: calcite, plagioclase, or iron hydroxide. The laboratory-determined rate laws, such as the rate law of Chou and co-workers (CHOU et al., 1989) for calcite dissolution, only apply within the grid cells containing the cylinder wall, that is, at the mineral-water interface where the reactions actually take place. The local reactive surface area is calculated from the geometry of the pore, with $A_{grid} = 2\pi R\Delta y$, where Δy is the grid spacing in the axial direction. Thus, the total surface is $A_{tot} = 2\pi RL$, where L is the length of the pore. The dissolution at the pore wall, coupled with a rigorous representation of the flow and diffusive transport, captures the dynamic reactive transport processes within a pore, even if the geometry is highly idealized. Reaction products from dissolution are swept and diffused downstream in the *y* (axial) direction, but also radially toward the center of the pore via molecular diffusion (Figure 1A). Multicomponent molecular diffusion is treated as a combination of Fickian diffusion of individual species and an electrochemical migration term arising from the diffusion of charged species at differing rates (LASAGA, 1998; NEWMAN, 1991; OELKERS, 1996; STEEFEL, 2007b). Hydrodynamic dispersion is not considered as a separate process, since this effect is captured rigorously through the combination of the parabolic velocity field and molecular diffusion (TAYLOR, 1953). All calculations are carried out with the code CrunchFlow (STEEFEL, 2007a).

Due to the coupling between flow, transport, and reactions, the aqueous concentrations at the outlet can vary as a function of radial distance. The averaged outlet concentration can be calculated as follows:

$$c_{out} = \frac{\int_0^R c(r)Q(r)}{Q_{tot}}, \tag{13}$$

where Q_{tot} is the total flow rate defined by

$$Q_{tot} = \int_o^R Q(r), \tag{14}$$

and c_{out} is the flux-weighted average concentration at the pore outlet, $c(r)$ is the concentration at radial distance r, and $Q(r)$ is the flow rate at radial distance r. The averaged outlet concentration depends on local dissolution rates at the pore wall, the advective transport along the axis of the pore, and the diffusive transport in both the axial and transverse directions. The overall reaction rate within the pore, R_{2D}, is calculated from the flux-weighted average of concentrations in the outlet solution, that is, the effluent chemistry. Based on the mass balance of the pore, the averaged area-normalized dissolution rate within the pore R_{2D} can be calculated as follows:

$$R_{2D} = \frac{(c_{out} - c_{in})Q_{tot}}{A_{tot}}, \tag{15}$$

where c_{in} is the inlet concentration. Like the concentration field, the value of R_{2D} is also a function of coupling between flow, transport, and dissolution at the pore wall.

While a cylindrical pore is an idealized model of a natural pore, it captures the important first order effects, including the fact that flow is slower close to the mineral surface, an important feature of transport within a pore that affects the extent of mixing. In single pores, the conditions under which concentration gradients develop depend on the relative rates of flow, transport, and reactions. In the case where the reaction rate is fast enough relative to transport to change the aqueous chemistry of the pore, the tendency to develop concentration gradients within the pore depends on the effectiveness of molecular diffusion relative to flow—where flow is sufficiently rapid compared to molecular diffusion over the length scales of the single pore, concentrations within the pore will not be uniform and dissolution rates depend on the scale over which the concentration, and thus the reaction rate, are averaged.

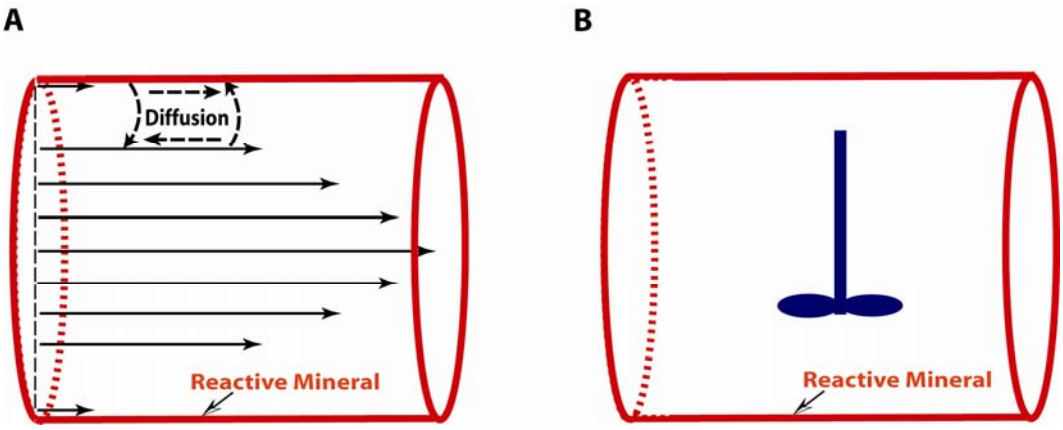

Figure 1: A.: Conceptual model for the Poiseuille Flow model, which considers reactive flow and transport in a single axi-symmetric cylindrical pore. The velocity profile is taken from the analytical solution for Poiseuille flow in a cylinder (DAUGHERTY and FRANZINI, 1965). B.: Conceptual model for the Well-Mixed Reactor model. Comparison of the rates from the two models quantifies the effects of mixing through molecular diffusion in both the transverse and longitudinal directions.

Well-Mixed Reactor model:

A Well-Mixed Reactor model for a single pore (Figure 1B) is developed for comparative purposes, since it allows us to quantify the extent to which concentration gradients captured by the Poiseuille Flow model affect the averaged reaction rates within a single pore. The pore represented in the Well-Mixed Reactor model possesses the same physical and chemical properties as that of the Poiseuille Flow pore, including total volume, reactive surface area, and total flow rate, except for the assumption that a rapid mixing rate ensures that there is no diffusion limitation on the rate—thus, the rate, R_M, is equivalent to what would be the case *if* the single pore behaved as a well-stirred laboratory reactor (Figure 1B). Under such conditions, the rate can be calculated from the laboratory-measured rate law using the equations in Section 2 and the uniform concentrations within the well-mixed pore.

The ratio of the rate from the well-mixed model, R_M, over R_{2D} is used to quantify the rate discrepancy between a natural pore and a well-mixed reactor. A ratio close to one indicates that the discrepancy in rates is negligible, that is, the pore is behaving effectively as a well-mixed

reactor. In contrast, a ratio significantly different from one implies that rates in natural pores and well-mixed reactors are not the same.

3.2 Models for a single fracture

Since the length of a single fracture can be considerably longer than the width of its aperture (in contrast to the geometry of a single pore), the effects of transverse and longitudinal mixing need to be assessed separately. As such, we consider an additional model, a 1D Plug Flow Reactor model, which is designed to quantify the effect of transverse mixing within the fracture. The other two, the Poiseuille Flow and Well-Mixed Reactor models differ only geometrically from those considered for the cylindrical pore described above.

Poiseuille Flow model:

Conceptually, single fractures are represented by two parallel plates. The distance between the two plates is the fracture aperture. The flow field within a fracture is represented by the Poiseuille flow between two parallel plates:

$$u(x) = 1.5U\left[1 - \left(\frac{x}{\delta}\right)^2\right], \qquad (16)$$

where $u(x)$ is the local fluid velocity within the fracture, U is the average flow velocity, x is the transverse distance to the center of a fracture, and δ is the half fracture aperture. As in the case of the single pore model, dissolution occurs only at the fracture wall, so that the laboratory-measured rate laws are applied only at the fracture wall itself.

By discretizing the fracture in both the transverse and longitudinal directions, we make no a priori assumption about the extent of mixing in either direction. The extent of mixing is determined by molecular diffusion, which is calculated numerically within the model. As with the cylindrical pore, dispersion is not explicitly considered in the model, other than by the combination of the detailed parabolic flow field and the longitudinal and transverse molecular diffusion. Overall reaction rates (R_{2D}) are calculated from the flux-weighted average of outlet concentrations in a similar fashion to the single pore model (Equation 15).

1D Plug-Flow Reactor model:

Since the fracture length can be much larger than the fracture aperture, the fracture can also be represented by a 1D Plug-Flow Reactor model in which the longitudinal direction is discretized, while complete mixing in the transverse direction is assumed. The result is a one-dimensional model that does not consider the parabolic velocity profile within the fracture. Overall rates from the 1D model (R_{1D}) are calculated from the concentrations of outlet solution (in this model, now represented by a single grid cell, in contrast to the 2D case). Comparison between R_{2D} and R_{1D} quantifies the effects of transverse mixing.

Well-Mixed Reactor model:

As in the case of a single cylindrical pore, the Well-Mixed Reactor model for the fractures assumes complete mixing in both transverse and longitudinal directions. The overall rates (R_M) are also calculated from the concentrations of fracture effluent. Comparison between R_{2D} and R_M

provides a measure of the combined effects of transverse and longitudinal mixing, while comparison between R_{1D} and R_M is a measure of the effects of longitudinal mixing.

4. Validation and verification of the Poiseuille Flow model

4.1 Verification of transport for the cylindrical pore

The numerical model implemented in CrunchFlow is verified against an analytical solution for Taylor dispersion (TAYLOR, 1953). Using Equation (12) for the flow field within a cylindrical pore, Taylor derived an analytical expression for hydrodynamic dispersion in the case of Poiseuille flow (TAYLOR, 1953)

$$D_h = D + \frac{UR^2}{D}, \tag{17}$$

where D_h is the dispersion coefficient, and D is the molecular diffusion coefficient. Note that the molecular diffusion coefficient appears both in the first term on the right hand side of Equation (17), where it contributes to dispersion in the longitudinal or axial direction, and in the denominator of the second term, where it counteracts the dispersion attributable to the variation in velocity within the pore.

Figure 2 shows a comparison between the breakthrough curve for a non-reactive tracer calculated with a one dimensional geometry using the Taylor-Aris dispersion coefficient given in Equation (17) and a two-dimensional axi-symmetric cylindrical Poiseuille flow calculation where dispersion is represented only through the variation in flow velocities and molecular diffusion. The excellent agreement indicates that the numerical code CrunchFlow captures the transport within the pore rigorously.

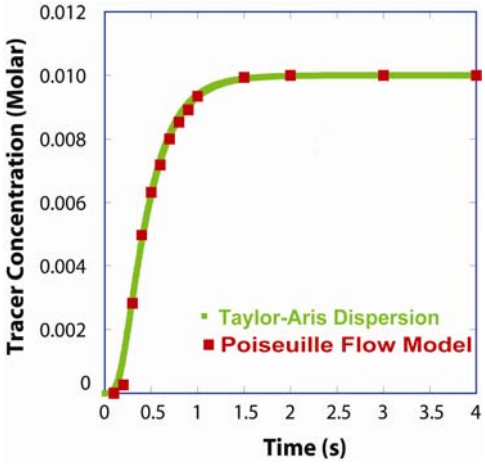

Figure 2: Comparison of non-reactive tracer breakthrough curves calculated with a one-dimensional geometry using an analytical Taylor-Aris dispersion coefficient (TAYLOR, 1953) and a full two-dimensional numerical calculation of transport in a cylinder using the code CrunchFlow.

4.2 Validation with a microfluidic reactive flow experiment

To validate the cylindrical pore model, a microfluidic reactive flow experiment was carried out using a 500 μm diameter and 4000 μm long cylindrical pore drilled in a single crystal of calcite

(Figure 3A). Single crystals of calcite (Iceland spar) were cut into 20 mm (L) by 10 mm (W) slabs and polished down to the thickness of 4 mm. A single 500 μm diameter cylindrical pore was drilled through the center of the polished sample sandwiched between two protecting ceramic plates (100 μm thickness). Nanoport® assemblies (Upchurch Scientific) were attached to the protecting ceramic plates for transferring fluids in and out of the calcite single pore. Input solutions were prepared using deionized water (18.3 Megohm-cm) and were adjusted to the desired pH with diluted ultrapure HNO_3 acid (J. T. Baker®). The ionic strength of input solutions was adjusted to 10 mM with reagent grade NaCl (Omnipure® from EMD). The output solution pH was measured with Orion® micro-pH electrode. All effluent samples were acidified with 2% ultrapure HNO_3 and analyzed in triplicate by inductive coupled plasma-optical emission spectrometer (ICP-OES, Perkin-Elmer 5300 DV model) with a micro-PFA nebulizer.

Solutions at pH 4 and 5 were injected into the pore with a syringe pump at two different flow rates, 4.72 μL/min and 9.39 μL/min. These flow rates result in average velocities of 0.04 cm/sec and 0.08 cm/sec, respectively. Figure 3B compares the flux-weighted average concentration of Ca^{2+} calculated from the Poiseuille Flow model for the cylindrical pore to the measured Ca^{2+} concentration from the microfluidic experiment at steady-state under two pH and flow conditions. Note that the reactive surface area is calculated in the grid cells along the cylinder wall from $A_{grid} = 2\pi R\Delta y$, where Δy is the grid spacing in the axial direction. The rate law of Chou and Wollast (CHOU et al., 1989) is assumed at the mineral-water interface, that is, within the grid cells containing the cylinder wall.

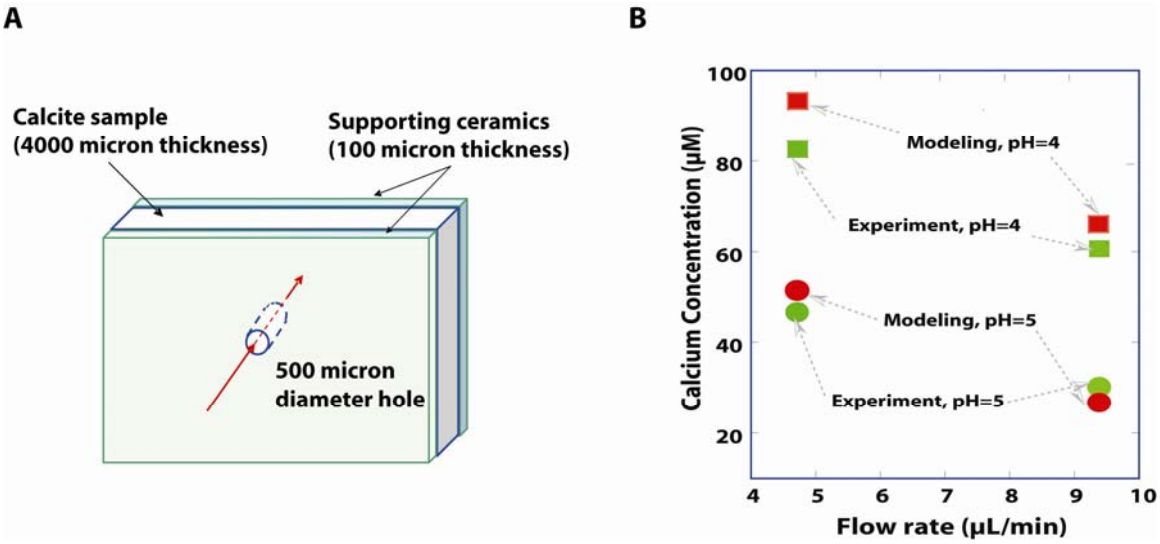

Figure 3. A. Schematic representation of the microfluidic reactive flow experiment. B. Comparison of the flux-weighted average concentration of Ca^{2+} calculated from the numerical Poiseuille Flow model and the measured Ca^{2+} concentration from the outlet of the microfluidic reactive flow experiment under two pH and flow conditions. The numerical model uses a flow field based on Poiseuille's Law (DAUGHERTY and FRANZINI, 1965) and a calcite dissolution rate law from Chou et al (CHOU et al., 1989) that is applied at the mineral-water interface (the pore wall). The simulation results match the experimental data well, thus validating the numerical model.

5. Results

5.1 Development of concentration gradients at the pore scale

To illustrate the effects of coupling between flow, transport, and reaction on the scale dependence of reaction rates (and thus to discrepancies between lab and field rates that may be due to processes operating at the pore scale), we show a concentration field that develops within a calcite pore of 100 μm in length at a flow velocity of 0.1 cm/s. The pore is infiltrated by a dilute pH 5 solution undersaturated with respect to the calcite, thus dissolving it. Under slightly acidic conditions, the dissolution of the calcite raises the pH and calcium concentration in the solution. The increase in pH resulting from calcite dissolution has the effect of creating a wedge-shaped, higher pH zone in the direction of flow that broadens as a result of molecular diffusion (Figure 4). Although not shown in the figure, similar concentration gradients for other species, such as Ca^{2+} and H_2CO_3, also develop within the cylindrical pore. In this physical setting, if molecular diffusion were absent, the pH effects would be restricted to the immediate vicinity of the calcite surface along the pore wall.

Now as gradients in pH develop, it should be clear that the scale at which the solution in the pore is sampled determines the calcite dissolution rate that is calculated—for example, a microelectrode pH measurement from a small volume close to the calcite pore wall (Box 1 in Figure 4) would indicate a dissolution rate greater than a pH measurement taken in a similarly sized volume in the center of the pore (Box 2 in Figure 4). In the same way, a sample volume extending over the entire end of the pore (Box 3 in Figure 4), as in the case where effluent from the entire pore is sampled, represents an average of more concentrated and less concentrated solution. As a result, the bulk dissolution rate from the cylindrical pore, R_{2D}, calculated from the flux-weighted effluent concentration, does not necessarily represent the reaction progress at the immediate vicinity of the mineral surface, and therefore is scale dependent.

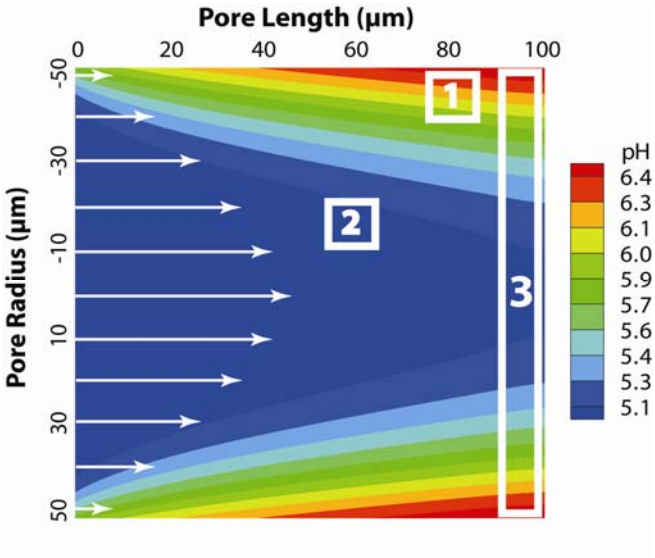

Figure 4. Contour plot of pH for a cross section of a pore of 100 μm in length and in diameter, with a pH 5 solution injected at a rate of 0.1 cm/s. The dissolution rate is scale dependent, as is clear from comparing different sample volumes: Box 1 represents a micro-sample volume close to the pore wall showing a higher pH (and calcium

concentration) than does Box 2 in the center of the pore, while Box 3, which averages the concentrations over the entire diameter of the pore, represents the pH that would be sampled as effluent.

5.2 Single pore results

To map out the conditions under which scale-dependent rates at the pore scale may develop, we modeled calcite, plagioclase, iron hydroxide dissolution under various hydrodynamic and pore size conditions. For all simulations, the pores were chosen to have equal values of diameter and length. Three pore sizes, 10 μm, 100 μm, and 1000 μm, were chosen that correspond to a range in size from relatively small pores in sandstones or clay-rich material (ACHARYA et al., 2005) to large pores in coarse-textured sediments or sandy soil (HWANG II and POWERS, 2003; KHALEEL and HELLER, 2003; KHALEEL and RELYEA, 2001). For each pore size, the pore flow velocity was varied from 10^{5} to 10^{-5} cm/s corresponding to Darcy velocities from 10^{4} to 10^{-6} cm/s for a porous medium of porosity equal to 0.1. The high flow velocities may be achieved in permeable aquifers in the vicinity of a pumping well, but otherwise are not common. All simulations were carried out at Reynolds numbers below where turbulence typically begins. The pH of the inlet solution was fixed at 5, representing the slightly acidic conditions that may be encountered in geological sequestration of CO_2 in deep aquifers (KNAUSS et al., 2005).

In general, calcite dissolution rates in both models increase with increasing pore flow velocity, as shown in Figure 5. With slow flow velocities (slower than 0.1 cm/s), the long residence times allow diffusion to homogenize the concentration field, thus producing results that match those of the Well-Mixed Reactor model (see left panel of Figure 5). With fast flow velocities (greater than 1000 cm/s), there is insufficient reaction to alter the pH even in areas close to the pore wall. This results in a uniform concentration field across the pore, again similar in this respect to the results from the Well-Mixed Reactor model (see right panel of Figure 5). Only where reaction and advection rates are comparable, as is the case with moderate flow velocities, can large concentration gradients develop (as shown in the middle panel of Figure 5). Under these conditions, the rate discrepancy between the two models is at its maximum.

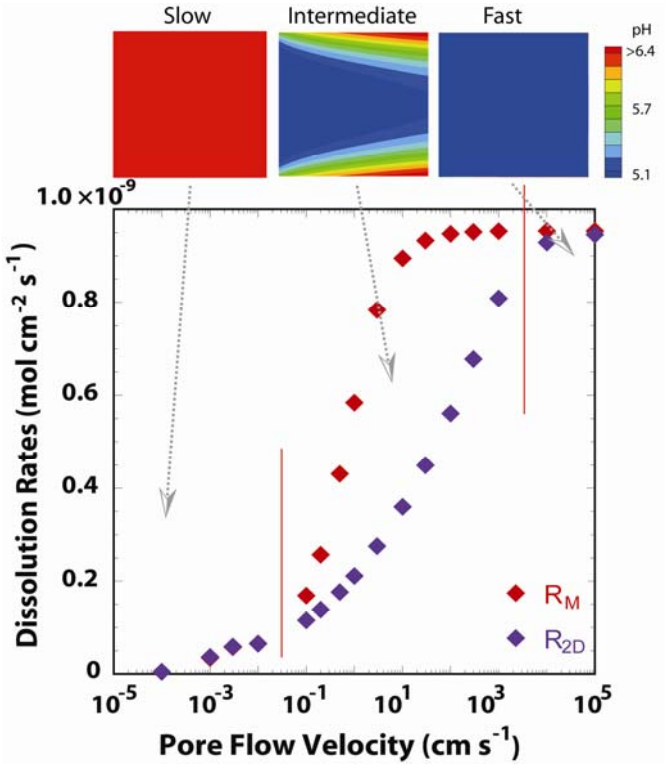

Figure 5. Comparison of calcite dissolution rates calculated from the Poiseuille Flow model (R_{2D}) and those from the Well-Mixed Reactor model (R_M) as a function of the pore flow velocity for a pore of 100 µm length and diameter. The rate discrepancy is negligible under fast and slow flow conditions, where the reactions are surface-controlled and transport controlled, respectively. The discrepancy is at its maximum under mixed surface reaction and transport controlled conditions where the rates of dissolution and transport are comparable. The upper panels show contour plots of pH for a cross section of a cylindrical pore of 100 µm in length and diameter under slow (left panel), intermediate (middle panel), and fast (right panel) flow velocities. Under both slow and fast flow conditions the pH fields are homogeneous, as is the case in a well-mixed laboratory reactor. Only under intermediate flow conditions where concentration gradients develop do the reaction rates depend on the spatial scale and the rate discrepancy between the two models reaches a maximum.

Not surprisingly, the scaling effect, indicated by the deviation of the ratio of R_M over R_{2D} from unity, varies with flow velocity. At low and high flow velocities, the homogeneous concentration field makes the scaling effect negligible, with ratios of R_M over R_{2D} close to unity; under medium flow conditions, the scaling effect reaches a maximum. The scaling effect also increases with increasing pore size due to the lack of complete mixing within large pores, as shown in Figure 6. With large pores (1000 µm), the ratio of R_M over R_{2D} can reach as high as 7, while with small pores (10 µm), the maximum ratio is only 1.3.

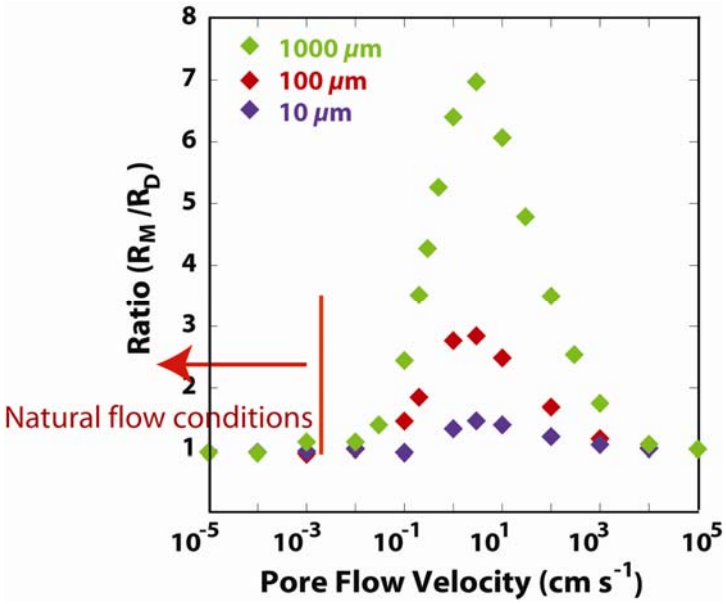

Figure 6. The scaling effect in a single pore, quantified by the ratio of R_M / R_{2D}, under various flow conditions, and for three pore sizes, 1000 μm, 100 μm, and 10 μm. The scaling effect is largest under intermediate flow and large pore conditions.

For both plagioclase and iron hydroxide pores, the pH profiles are uniform under all pore size and flow conditions, with pH values similar to that of the inlet solution. This is due to the fact that the dissolution rates of both plagioclase and iron hydroxide are so slow that their rates are much smaller than advection and diffusion under all conditions over the length scale of a single pore, thus leading to homogeneous concentration fields. The rate discrepancy at this scale is therefore negligible under all conditions in the case of these minerals.

At the pore scale, a discrepancy in rate between the Poiseuille Flow model and the Well-Mixed Flow model occurs in the case of calcite under flow conditions between 0.1 to 1000 cm/s. Under natural flow conditions where flow velocities are typically less than 0.001 cm/s, however, mixing via molecular diffusion is effective in homogenizing the concentration field, thus eliminating any discrepancies between the Poiseuille Flow and the Well-Mixed Reactor model. This suggests that a scale dependence to mineral dissolution rates is unlikely at the single pore or fracture scale under normal geological/hydrologic conditions, implying that the discrepancy between laboratory and field rates must be attributed to other factors.

5.2 Single fracture results

Although the size of fracture aperture can range from microns to hundreds of microns (STEEFEL and LASAGA, 1994), here we chose to examine a fracture of an intermediate aperture size of 100 μm, while its length is allowed to vary from tens of microns to one centimeter. This allows us to examine the extent to which fracture length affects any potential rate discrepancy. The flow conditions were chosen based on typical head gradients in field settings, permeability values for fractured rocks (FREEZE and CHERRY, 1979), and a fracture spacing of 0.1 m. These values give a flow velocity range of 10^{-1} to 10^{-5} cm/s. Here we detail the results for a flow

velocity of 0.1 cm/s. The composition of the inlet solution is the same as that for the single pore simulations.

Figure 7 shows the concentration fields for relevant species and pH for all three reactions for a fracture of 0.24 cm in length. Due to the fact that dissolution occurs at the fracture wall, concentrations of Ca^{2+} and Fe^{2+} are highest here and become progressively lower toward the center of the fracture. The contour plot of the Ca^{2+} and Fe^{2+} concentration fields look similar for all three reactions, since the geometry is determined primarily by the relative rate of flow and diffusion for a given fracture aperture, δ, or the Péclet number, given by (STEEFEL and LICHTNER, 1998)

$$Pe = \frac{v\delta}{D}. \qquad (18)$$

However, due to the significant differences in the magnitude of reaction rates, the extent of reaction is very different for the three reactions. With calcite dissolution, the Ca^{2+} concentration increases to about 10^{-5} mol/L, while for plagioclase and iron dissolution, the Ca^{2+} and Fe^{2+} concentrations only increase to about 10^{-9} mol/L. As a result, the pH values cover four pH units for calcite dissolution, while the pH change is negligible for both plagioclase and iron dissolution (on the order of 0.0001 to 0.001 pH unit), thus resulting in an essentially homogeneous pH field.

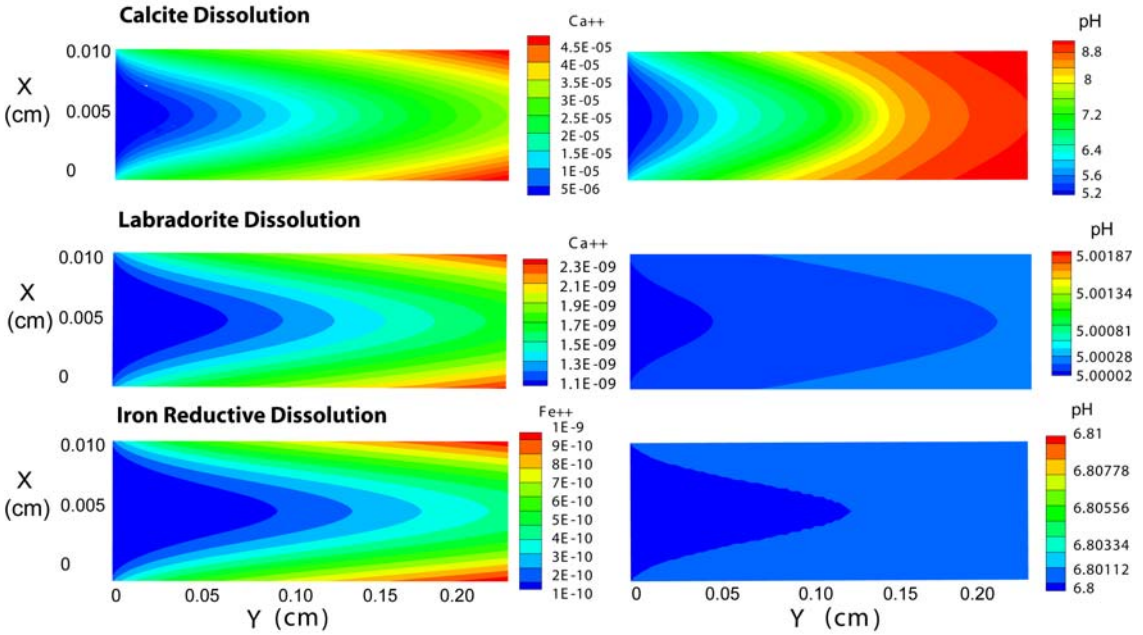

Figure 7: Concentration fields of relevant species for calcite dissolution, plagioclase dissolution, and iron reductive dissolution in a fracture with an aperture of 100 µm and a length of 0.24 cm. The flow velocity is 0.1 cm/s. The Ca^{2+} and Fe^{2+} concentration fields look similar in terms of their shape, since this is determined by the relative rate of flow and diffusion. However, the extent of reaction differs significantly for the three minerals because of the difference in rates, an observation that is confirmed by the large change in pH values in the calcite fracture compared to the negligible pH change in the plagioclase and iron hydroxide fractures.

Calcite

The flux-weighted average of the calcite dissolution rates from each of the three models decrease as the fracture length increases, as shown in Figure 8A. This is largely due to the nonlinear coupling between dissolution rates and pH, as well as the associated spatial variation in dissolution rates along the fracture wall. The pH is lowest and therefore the dissolution rates are fastest close to the fracture inlet. As mineral dissolution increases pH, it also decreases dissolution rates downstream, as can be seen from Figure 9. Within a fracture of 0.24 cm in length, pH increases by more than four units and the dissolution rates drop almost an order of magnitude. After pH drops to a value of about 7, the rate becomes constant because the rate is independent of pH, as indicated in Equation 4. The result is that the averaged rates from the models decrease with increasing fracture length.

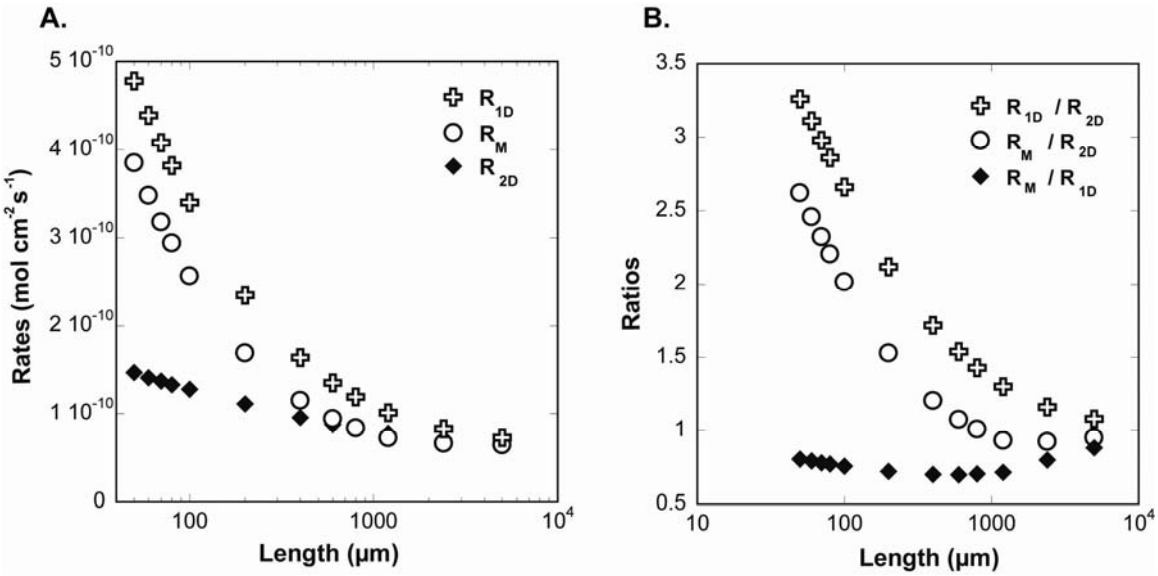

Figure 8: A. Flux-weighted average reaction rates as a function of calcite fracture length, from the Poiseuille Flow model that fully couples the reactive transport processes (R_{2D}), the 1D Plug Flow Reactor model that assumes complete transverse mixing (R_{1D}), and the Well-Mixed Reactor model that assumes complete mixing in both longitudinal and transverse directions (R_M). B. Comparison between flux-weighted average rates calculated from the three models. The ratio of R_{1D} over R_{2D} is a measure of the effects of transverse mixing; the ratio of R_M over R_{2D} is a measure of the combined effects of transverse and longitudinal mixing; and the ratio of R_M over R_{1D} indicates the effects of longitudinal mixing.

The ratios of the flux-weighted average calcite dissolution rates from the three models are also a function of the fracture length, as shown in Figure 8B. As mentioned above, the ratio of R_{1D} over R_{2D} quantifies the effects of transverse mixing, the ratio of R_M over R_{2D} measures the combined effects of transverse and longitudinal mixing, while the ratio of R_M over R_{1D}

indicates the effect of longitudinal mixing.

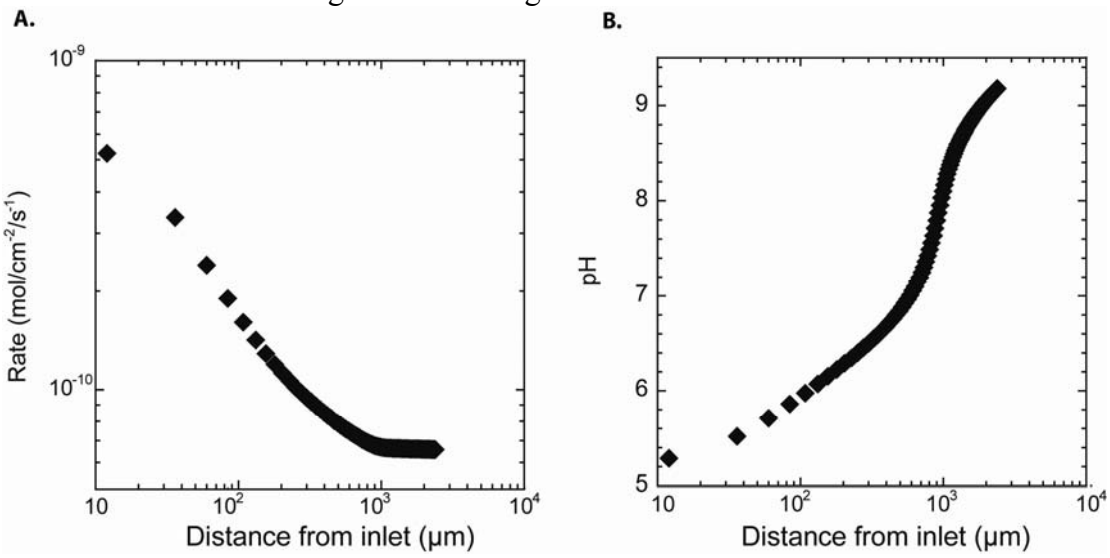

Figure 9: A. Calcite dissolution rates and pH at the fracture wall as a function of distance from the inlet for a fracture of length 0.24 cm. Dissolution rates decrease rapidly close to the inlet due to the pH dependence and high reaction rates there. After the pH increases to about 7, dissolution rates become constant as the rate becomes independent of pH.

From Figure 8B, it is interesting to notice that the effects of transverse mixing are much larger than the effects of longitudinal mixing, as the deviation of R_{1D} / R_{2D} from unity is much larger than that of R_M / R_{1D}. The assumption of complete transverse mixing in the 1D model leads to an overestimation of reaction rates by a factor of 3.3 in a 50 μm long fracture. The assumption of complete longitudinal mixing leads to an underestimation of reaction rates by the Well-Mixed Reactor model. As a result of the opposite direction of the effects of the transverse and longitudinal mixing, the ratio of R_M over R_{2D}, which combines the two effects, falls in between the ratios of R_{1D} / R_{2D} and R_M / R_{1D}.

In all cases, the deviation from unity decreases with increasing length and the rates from the three models converge as longer fractures are considered. There are two reasons for this behavior. First, the fast dissolution rates at the fracture inlet leads to maximum concentration gradients in the transverse direction--while the Ca^{2+} concentration at the fracture wall is of the order of 10^{-5} mol/L, at the center of the fracture the Ca^{2+} concentration is very low, essentially the same as the inlet solution. As a result, most of the aqueous solution within a short fracture does not show significant reaction progress except in the immediate vicinity of the pore wall. With long fractures, however, molecular diffusion has more time to spread the Ca^{2+} from the fracture wall to its center, and the solution within the fracture becomes more nearly homogeneous. For example, at the outlet of a 0.24 long fracture, the Ca^{2+} concentrations at the fracture wall and the fracture center are of the same order of magnitude. Second, the dissolution rates at the fracture wall become constant once the fracture length is larger than 0.1 cm as a result of the increase in pH. As a result, scaling effects tend to diminish in the case of longer fractures.

This result suggests that for fast reactions such as calcite, the scaling effects can be large when the length scale of the fracture is small, and the scaling effects diminish with increasing fracture length. This is interesting in the sense that it is different from the case of dispersion in hierarchical porous media, where scaling effects increase with increasing length scale (GELHAR et al., 1992).

Plagioclase

For plagioclase, the overall dissolution rates also decrease with increasing fracture length, as shown in Figure 10A for rates calculated using aluminum inhibition rate law proposed by OELKERS et al (1994). However, due to the slowness of the plagioclase dissolution rate, there is little change in concentration and the fracture remains nearly homogeneous. As such, all three models give similar reaction rates, and the rate discrepancies are negligible compared to calcite dissolution, as shown in Figure 10B. It is interesting to note that for plagioclase dissolution, the effects of transverse mixing are much smaller than those due to longitudinal mixing, as the ratios of R_{1D}/R_{2D} are all close to unity, while the ratios of R_M/R_{1D} deviates from unity slightly. This is primarily because plagioclase dissolution is so slow that significant concentration gradients do not develop in the transverse direction. It is also worth noting that the ratio of R_M/R_{1D} deviates from unity increasingly with increasing fracture length, meaning that the effects of longitudinal mixing become progressively more significant with increasing fracture length. This is particularly true for the aluminum inhibition rate law suggested by OELKERS et al. (1994), since complete mixing in the longitudinal direction results in higher aluminum concentrations close to the fracture inlet, and thus to slower overall rates. Simulations using the rate law proposed by HELLMANN and TISSERAND (2006) give similar results.

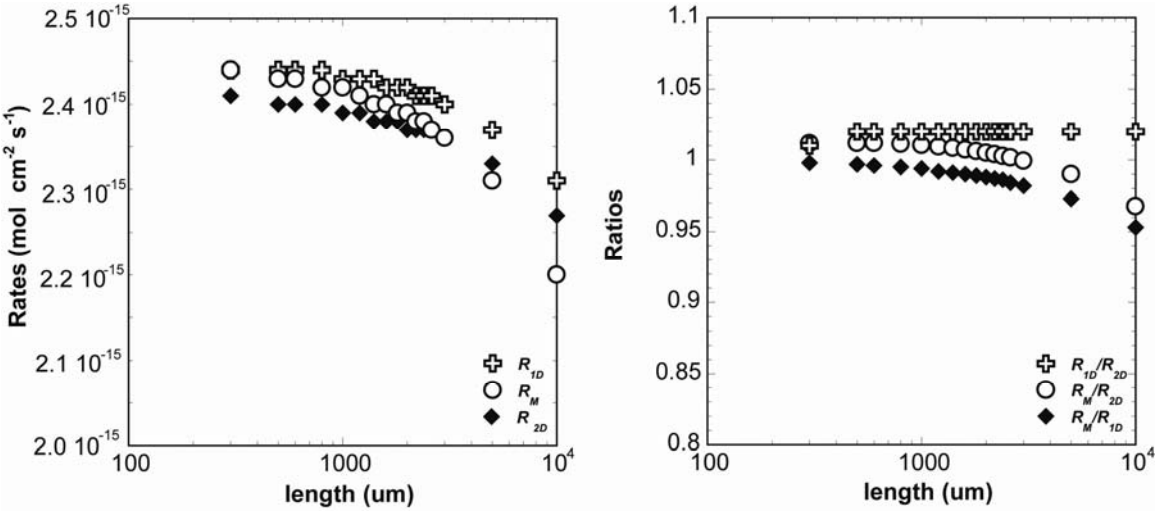

Figure 10: A. Overall plagioclase dissolution rates calculated as a flux-weighted average at the fracture outlet from the three models as a function of fracture length: the Poiseuille Flow model (R_{2D}), the 1D Plug Flow Reactor model (R_{1D}), and the Well-Mixed Reactor model (R_M). B. The comparison of rates from different models. Rates from all three models look similar, with ratios close to unity. However, the effects of longitudinal mixing (R_M/R_{1D}) are larger than that of transverse mixing (R_{1D}/R_{2D}).

6. Discussion

Overall, the results show that a scale dependence to mineral dissolution rates, leading potentially to a discrepancy between laboratory and field rates, arises when large concentration gradients develop, a situation that is inherently different from the well mixed laboratory conditions where most mineral reaction rates are measured. Time scale analysis reveals that steep concentration profiles only occur under two necessary conditions. First, the rates of advection and reaction must be similar so that aqueous concentrations of involved species can change significantly within a pore. Second, diffusion must be slower than advection so that it cannot eliminate the spatial gradients in concentration within the pore. This implies that it is only in transport regimes where homogeneous concentration fields form that laboratory-measured reaction rates be used directly This is consistent with findings from other studies at other spatial scales (MEILE and TUNCAY, 2006; MO and FRIEDLY, 2000; MOHAMED et al., 2006) where it was demonstrated that relatively fast reaction kinetics combined with low advection and diffusion rates can generate a scaling effect, and thus a discrepancy between lab and field rates.

While the above results are based on idealized single pore and single fracture models, its validity is probably even stronger in natural porous media. The cylindrical pore, with only two openings and smooth mineral surfaces, represents an extreme condition with a minimum extent of mixing. In contrast, natural porous media typically have a larger number of openings (LINDQUIST et al., 2000) and rough mineral surfaces, both of which can increase the extent of mixing and reduce the rate discrepancy due to incomplete mixing. Under natural conditions, it is also likely that reactive minerals are heterogeneously distributed along the pore wall. However, to the extent that molecular diffusion is effective in homogenizing the pore, the heterogeneity of the reactive mineral distribution is not going to play a role in creating a scale dependence at this scale.

Although under natural conditions the rate discrepancies are considered to be negligible at the scale of single pores and fractures, at larger spatial scales these effects are expected to become more significant. The characteristic time for diffusion or dispersion to homogenize a concentration field is proportional to the square of the length scale and therefore increases rapidly with increasing spatial scale. As such, the conditions for rate discrepancy to appear are more easily encountered. Field measurements of dissolution rates are often carried out at much larger spatial scales than the pore scale (ZHU, 2005), which may provide an explanation for the consistent emergence of the scaling issue and lab-field rate discrepancies.

7. Conclusions

In summary, we examined the effects of flow and transport processes on mineral dissolution kinetics in single pores and fractures. Laboratory-measured reaction kinetics were coupled with Poiseuille flow and advective and diffusive transport to unravel some of mechanisms that might contribute to a scale dependence of the reaction rates, and thus to a discrepancy between laboratory and field rates. The simulations were intended to identify the conditions under which such a rate discrepancy becomes significant at the pore scale by comparing the results with a well-mixed pore where pore-scale transport processes are ignored.

Single pore simulation results show that rate discrepancies arise primarily as a result of the formation of concentration gradients, which develop due to comparable rates of reaction and advective transport, and incomplete mixing via molecular diffusion. As a result, the magnitude of the reaction rates plays a large role in determining the scaling behavior of reaction rates. For calcite dissolution, the rate discrepancy becomes significant at flow velocities between 0.1 cm/s and 1000 cm/s, while the discrepancy is negligible at slower or faster flow rates. In the case of plagioclase dissolution and Fe reductive dissolution, the rates are too slow to register a significant effect at the higher flow rates where molecular diffusion does not dominate. Under natural conditions where flow velocities are typically lower than 0.001 cm/s, molecular diffusion homogenizes the concentration fields, and even the rate discrepancy for calcite dissolution disappears. As such, we conclude that for single pores, the discrepancy between the rate determined with the flux-weighted average at the pore outlet and the rate calculated assuming complete mixing is negligible. The individual pore or fracture, therefore, behaves effectively as a well-mixed reactor. We conclude therefore that the widely cited discrepancy between laboratory and field rates cannot be attributed to pore scale processes.

With longer fractures, we also examined the effects of length scale on the rate discrepancy and the effects of transverse and longitudinal mixing. Again, the magnitude of the reaction rates plays a large role in the extent of rate discrepancy. For the fast calcite dissolution, the effects of transverse mixing are more important than those due to longitudinal mixing, because the fast dissolution rates lead to large differences between concentration at the fracture wall and those at the fracture center. Rate discrepancies decrease with increasing fracture length in the case of calcite due to the combined effects of slower reaction rates downstream resulting from the increase in pH and as a result of the increased extent of mixing via molecular diffusion. For slow reactions of plagioclase and iron dissolution, although longitudinal mixing is more important, the effects are negligible within a spatial scale of one centimeter.

8. Acknowledgements

Funding was provided to the Center for Environmental Kinetics Analysis (CEKA) by the U.S. Department of Energy's Environmental Remediation Science Program as part of a joint NSF-DOE Environmental Molecular Science Institute at Pennsylvania State University. Additional funding was provided by the Laboratory-Directed Research and Development program at Lawrence Berkeley National Laboratory. We are grateful for the review of an early version of the manuscript provided by Dr. Donald DePaolo.

9. References

Acharya R. C., Van der Zee S., and Leijnse A. (2005) Transport modeling of nonlinearly adsorbing solutes in physically heterogeneous pore networks. *Water Resources Research* **41**(2).

Alekseyev V. A., Medvedeva L. S., Prisyagina N. I., Meshalkin S. S., and Balabin A. I. (1997) Change in the dissolution rates of alkali feldspars as a result of secondary mineral precipitation and approach to equilibrium. *Geochimica Cosmochimica Acta* **61**(6), 1125-1142.

Anbeek C. (1993) The Effect of Natural Weathering on Dissolution Rates. *Geochimica Et Cosmochimica Acta* **57**(21-22), 4963-4975.

Anderson R. T., Vrionis H. A., Ortiz-Bernad I., Resch C. T., Long P. E., Dayvault R., Karp K., Marutzky S., Metzler D. R., Peacock A., White D. C., Lowe M., and Lovley D. R. (2003) Stimulating the in situ activity of Geobacter species to remove uranium from the groundwater of a uranium-contaminated aquifer. *Applied and Environmental Microbiology* **69**(10), 5884-5891.

Appelo C. A. J., Van der Weiden M. J. J., Tournassat C., and Charlet L. (2002) Surface complexation of ferrous iron and carbonate on ferrihydrite and the mobilization of arsenic. *Environmental Science & Technology* **36**(14), 3096-3103.

Bear J. (1972) *Dynamics of Fluids in Porous media*. Dover Publications, Inc.

Berner R. A. (1995) Chemical weathering and its effect on atmospheric CO_2 and climate. In *Chemical Weathering Rates of Silicate Minerals*, Vol. 31, pp. 565-583.

Berner R. A. and Berner E. K. (1997) Silicate weathering and climate. In *Tectonics, Uplift and Climate Change* (ed. W. Ruddiman), pp. 353-365. Plenum.

Blum A. E. and Stillings L. L. (1995) Feldspar dissolution kinetics. In *Chemical Weathering Rates of Silicate Minerals*, Vol. 31 (ed. A. F. White and S. L. Brantley), pp. 291-351. Mineralogical Soc America.

Carroll S. A. and Knauss K. G. (2005) Dependence of labradorite dissolution kinetics on CO2(aq), Al(aq), and temperature. *Chemical Geology* **217**(3-4 SPEC. ISS.), 213-225.

Chorover J., Choi S. K., Amistadi M. K., Karthikeyan K. G., Crosson G., and Mueller K. T. (2003) Linking cesium and strontium uptake to kaolinite weathering in simulated tank waste leachate. *Environmental Science & Technology* **37**(10), 2200-2208.

Chou L., Garrels R. M., and Wollast R. (1989) Comparative study of the kinetics and mechanisms of dissolution of carbonate minerals. *Chemical Geology* **78**, 269 - 282.

Coates J. D. and Anderson R. T. (2000) Emerging techniques for anaerobic bioremediation of contaminated environments. *Trends in Biotechnology* **18**(10), 408-412.

Daugherty R. L. and Franzini J. B. (1965) *Fluid Mechanics with Engineering Applications*. McGraw-Hill.

Dzombak D. A. and Morel F. M. M. (1990) *Surface complexation modeling*. John Wiley and Sons.

Freeze R. A. and Cherry J. A. (1979) *Groundwater*. Prentice Hall, Inc.

Gelhar L. W., Welty C., and Rehfeldt K. R. (1992) A Critical-Review of Data on Field-Scale Dispersion in Aquifers. *Water Resources Research* **28**(7), 1955-1974.

Hwang II S. and Powers S. E. (2003) Lognormal distribution model for estimating soil water retention curves for sandy soils. *Soil Science* **168**(3), 156-166.
Jaisi D. P., Dong H. L., and Liu C. X. (2007) Influence of biogenic Fe(II) on the extent of microbial reduction of Fe(III) in clay minerals nontronite, illite, and chlorite. *Geochimica Et Cosmochimica Acta* **71**(5), 1145-1158.
Khaleel R. and Heller P. R. (2003) On the hydraulic properties of coarse-textured sediments at intermediate water contents. *Water Resources Research* **39**(9).
Khaleel R. and Relyea J. F. (2001) Variability of Gardner's alpha for coarse-textured sediments. *Water Resources Research* **37**(6), 1567-1575.
Knauss K. G., Johnson J. W., and Steefel C. I. (2005) Evaluation of the impact of CO_2, co-contaminant gas, aqueous fluid and reservoir rock interactions on the geologic sequestration of CO_2. *Chemical Geology* **217**, 339-350.
Lasaga A. C. (1998) *Kinetic theory in the earth sciences*. Princeton University Press.
Li L., Peters C. A., and Celia M. A. (2006) Upscaling geochemical reaction rates using pore-scale network modeling. *Advances in Water Resources* **29**(9), 1351-1370.
Li L., Peters C. A., and Celia M. A. (2007) Effects of mineral spatial distribution on reaction rates in porous media. *Water Resources Research* **43**(1).
Lindquist W. B., Venkatarangan A., Dunsmuir J., and Wong T. F. (2000) Pore and throat size distributions measured from synchrotron X- ray tomographic images of Fontainebleau sandstones. *J. Geophys. Res.-Sol. Ea.* **105**(B9), 21509-21527.
Liu C. X., Kota S., Zachara J. M., Fredrickson J. K., and Brinkman C. K. (2001) Kinetic analysis of the bacterial reduction of goethite. *Environmental Science & Technology* **35**(12), 2482-2490.
Lovley D. R. (1993) Dissimilatory Metal Reduction. *Annual Review of Microbiology* **47**, 263-290.
Lovley D. R. and Coates J. D. (1997) Bioremediation of metal contamination. *Current Opinion in Biotechnology* **8**(3), 285-289.
Maher K., DePaolo D. J., and Lin J. C. F. (2004) Rates of silicate dissolution in deep-sea sediment: In situ measurement using U-234/U-238 of pore fluids. *Geochimica Et Cosmochimica Acta* **68**(22), 4629-4648.
Maher K., Steefel C. I., DePaolo D. J., and Viani B. E. (2006) The mineral dissolution rate conundrum: Insights from reactive transport modeling of U isotopes and pore fluid chemistry in marine sediments. *Geochimica et Cosmochimica Acta* **70**(2), 337-363.
Malmstrom M. E., Destouni G., Banwart S. A., and Stromberg B. H. E. (2000) Resolving the Scale-Dependence of Mineral Weathering Rates. *Environmental Science & Technology* **34**(7), 1375-1378.
Malmstrom M. E., Destouni G., and Martinet P. (2004) Modeling expected solute concentration in randomly heterogeneous flow systems with multicomponent reactions. *Environ. Sci. Technol.* **38**, 2673-2679.
Meile C. and Tuncay K. (2006) Scale dependence of reaction rates in porous media. *Advances in Water Resources* **29**(1), 62-71.
Mo Z. and Friedly J. C. (2000) Local reaction and diffusion in porous media transport models. *Water Resources Research* **36**(2), 431-438.

Mohamed M. M. A., Hatfield K., and Hassan A. E. (2006) Monte Carlo evaluation of microbial-mediated contaminant reactions in heterogeneous aquifers. *Advances in Water Resources* **29**(8), 1123-1139.

Morse J. W. and Arvidson R. S. (2002) The dissolution kinetics of major sedimentary carbonate minerals. *Earth-Science Reviews* **58**(1-2), 51-84.

Newman J. S. (1991) *Electrochemical systems*. Prentice Hall.

Oelkers E. H. (1996) Physical and chemical properties of rocks and fluids for chemical mass transport calculations. In *Reactive Transport in Porous Media*, Vol. 34 (ed. C. I. S. P. C. Lichtner, and E. H. Oelkers), pp. 131-191. The Mineralogical Society of America.

Oelkers E. H., Schott J., and Devidal J.-L. (1994) The effect of aluminum, pH, and chemical affinity on the rates of aluminosilicate dissolution reactions. *Geochimica et Cosmochimica Acta* **58**(9), 2011-2024.

Plummer L. N., Wigley T. M. L., and Parkhurst D. L. (1978) The kinetics of calcite dissolution in CO22-water systems at 5 degree C to 60 degree C and 0.0 to 1.0 atm CO2. Am. J. Sci. 278, 179-216.

Roden E. E. (2004) Analysis of long-term bacterial vs. chemical Fe(III) oxide reduction kinetics. *Geochimica Et Cosmochimica Acta* **68**(15), 3205-3216.

Roden E. E. and Urrutia M. M. (2002) Influence of biogenic Fe(II) on bacterial crystalline Fe(III) oxide reduction. *Geomicrobiology Journal* **19**(2), 209-251.

Roden E. E., Urrutia M. M., and Mann C. J. (2000) Bacterial reductive dissolution of crystalline Fe(III) oxide in continuous-flow column reactors. *Applied and Environmental Microbiology* **66**(3), 1062-1065.

Roden E. E. and Zachara J. M. (1996) Microbial reduction of crystalline iron(III) oxides: Influence of oxide surface area and potential for cell growth. *Environmental Science & Technology* **30**(5), 1618-1628.

Scheibe T. D., Fang Y., Murray C. J., Roden E. E., Chen J., Chien Y.-J., Brooks S. C., and Hubbard S. S. (2006) Transport and biogeochemical reaction of metals in a physically and chemically heterogeneous aquifer. *Geosphere* **2**(4), doi: 10.1130/GES00029.1.

Spycher N. F., Sonnenthal E. L., and Apps J. A. (2003) Fluid flow and reactive transport around potential nuclear waste emplacement tunnels at Yucca Mountain, Nevada. *Journal of Contaminant Hydrology* **62-3**, 653-673.

Steefel C. I. (2007a) CrunchFlow User's Manual. Lawrence Berkeley National Laboratory.

Steefel C. I. (2007b) Geochemical kinetics and transport In *Kinetics of Water-Rock Interaction* (ed. J. Kubicki. S. Brantley, A. White), Springer (in press).

Steefel C. I., DePaolo D. J., and Lichtner P. C. (2005) Reactive transport modeling: An essential tool and a new research approach for the Earth Sciences. *Earth and Planetary Science Letters* **240**, 539-558.

Steefel C. I. and Lasaga A. C. (1994) A coupled model for transport of multiple chemical species and kinetic precipitation/dissolution reactions with application to reactive flow in single phase hydrothermal systems. *Am. J. Sci.* **294**, 529-592.

Steefel C. I. and Lichtner P. C. (1998) Multicomponent reactive transport in discrete fractures: I. Controls on reaction front geometry. *Journal of Hydrology* **209**(1-4), 186-199.

Steefel C. I. and Van Cappellen P. (1990) A new kinetic approach to modeling water-rock interaction: the role of nucleation, precursors, and Ostwald ripening. *Geochimica et Cosmochimica Acta* **54**(10), 2657-2677.

Stefansson A. (2001) Dissolution of primary minerals of basalt in natural waters: I. Calculation of mineral solubilities from 0 degree C to 350 degree C. *Chemical Geology* **172**(3-4), 225-250.

Taylor G. I. (1953) The dispersion of soluble matter in a solvent flowing through a tube. *Proc. Royal Society London Series A* **219**, 196-203.

White A. F. (1995) Chemical weathering rates of silicate minerals in soils. In *Chemical Weathering Rates of Silicate Minerals*, Vol. 31 (ed. A. F. White and S. L. Brantley), pp. 407-461. Mineralogical Society of America.

White A. F. and Brantley S. L. (1995) Chemical weathering rates of silicate minerals: An overview. In *Chemical Weathering Rates of Silicate Minerals*, Vol. 31 (ed. A. F. White and S. L. Brantley), pp. 1-22. Mineralogical Society of America.

White A. F. and Brantley S. L. (2003) The effect of time on the weathering of silicate minerals: why do weathering rates differ in the laboratory and field? *Chemical Geology* **202**(3-4), 479-506.

White A. F. and Peterson M. L. (1990) Role of Reactive-Surface-Area Characterization in Geochemical Kinetic-Models. *Acs Symposium Series* **416**, 461-475.

Zhu C. (2005) In situ feldspar dissolution rates in an aquifer. *Geochimica Et Cosmochimica Acta* **69**(6), 1435-1453.

Zhu C., Blum A. E., and Veblen D. (2004) Feldspar dissolution rates and clay precipitation in the Navajo aquifer at Black Mesa, Arizona, USA. *Water-Rock Interaction*, 895-899.